Effects of Laminate Architecture on Fracture Resistance of Sponge Biosilica: Lessons from Nature**

By *Ali Miserez, James C. Weaver, Philipp J. Thurner, Joanna Aizenberg, Yannicke Dauphin, Peter Fratzl, Daniel E. Morse,* and *Frank W. Zok**

Hexactinellid sponges are known for their ability to synthesize unusually long and highly flexible fibrous spicules, which serve as the building blocks of their skeletal systems. The spicules consist of a central core of monolithic hydrated silica, surrounded by alternating layers of hydrated silica and proteinaceous material. The principal objective of the present study is to ascertain the role of the latter laminate architecture in the material's resistance to both crack initiation and subsequent crack growth. This has been accomplished through indentation testing on the giant anchor spicule of *Monorhaphis chuni*, both in the laminated region and in the monolithic core, along with a theoretical analysis of deformation and cracking at indents. The latter suggests that the threshold load for crack initiation is proportional to K_c^4/E^2H where K_c is fracture toughness, E is Young's modulus, and H is hardness. Two key experimental results emerge. First, the load required to form well-defined radial cracks from a sharp indent in the laminated region is two orders of magnitude greater than that for the monolithic material. Secondly, its fracture toughness is about 2.5 times that of the monolith, whereas the modulus and hardness are about 20% lower. Combining the latter property values with the theoretical analysis, the predicted increase in the threshold load is a factor of about 80, broadly consistent with the experimental measurements.

[*] Prof. F. W. Zok, Dr. A. Miserez
Materials Department
University of California, Santa Barbara, CA 93106 (USA)
E-mail: zok@engineering.ucsb.edu

Prof. D. E. Morse, Dr. J. C. Weaver
Department of Molecular, Cellular and Developmental Biology
and Institute for Collaborative Biotechnologies
University of California, Santa Barbara, CA 93106 (USA)
E-mail: d_morse@lifesci.ucsb.edu

Dr. P. J. Thurner
Bioengineering Science Research Group
School of Engineering Science
University of Southampton
Highfield, Southampton, S017, 1BJ (U.K.)

Prof. J. Aizenberg
Harvard School of Engineering and Applied Sciences
Cambridge, MA 02138 (USA)

Dr. Y. Dauphin
University UMR IDES
University of Paris-Sud
Orsay, 91405 (France)

Prof. P. Fratzl
Department of Biomaterials
Max Planck Institute of Colloids and Interfaces
Potsdam 14424 (Germany)

1. Introduction

The skeletal spicules of hexactinellid sponges have proved to be useful model systems for investigating structure–function relationships in biological materials, with the ultimate goal of identifying design strategies for new synthetic materials. Although comprised principally of an intrinsically brittle material, the spicules are remarkably robust and strong.[1,2] Their performance has been attributed largely to the spicule architecture, which consists of alternating concentric rings of hydrated silica and a proteinaceous material.[3–6]

In many hexactinellid species, the spicules are circular in cross-section, consistent with their role in supporting transverse bending loads. Additionally, the thickness of the silica layers diminishes with radial distance from the core, thus yielding a minimum value at the location where the bending stress is a maximum: notably, the outer surface. For well-bonded laminated structures of this type, the tensile stress needed to cause cracking of an individual layer is proportional to $h^{-1/2}$, where h is layer thickness.[7] This scaling suggests that the layer thickness variation is the result of a growth adaptation for imparting increased bending strength to the spicules.

Improvements to this design strategy are seen in the giant anchor spicule of *Monorhaphis chuni*, a deep-sea sediment-dwelling hexactinellid sponge found in the Pacific and Indian Oceans. In contrast to the large numbers of fine spicules used to anchor other hexactinellids to the ocean floor,[8] the anchoring apparatus of *M. chuni* consists of a single giant spicule, up to 3 m long and nearly 1 cm in diameter

exhibits even a modest capacity for plastic deformation, a crack formed in an individual silica layer would be expected to arrest at the neighboring organic interlayers. In order for the fracture process to proceed, new cracks would then have to be nucleated in the adjacent silica layers. Because of the stochastic nature of brittle fracture, renucleation would generally occur at locations that are non-coplanar with the initial crack. Indeed, observations of broken spicules reveal stair-step fracture patterns consistent with such a sequential arrest and renucleation process.[1,3–5,9,10]
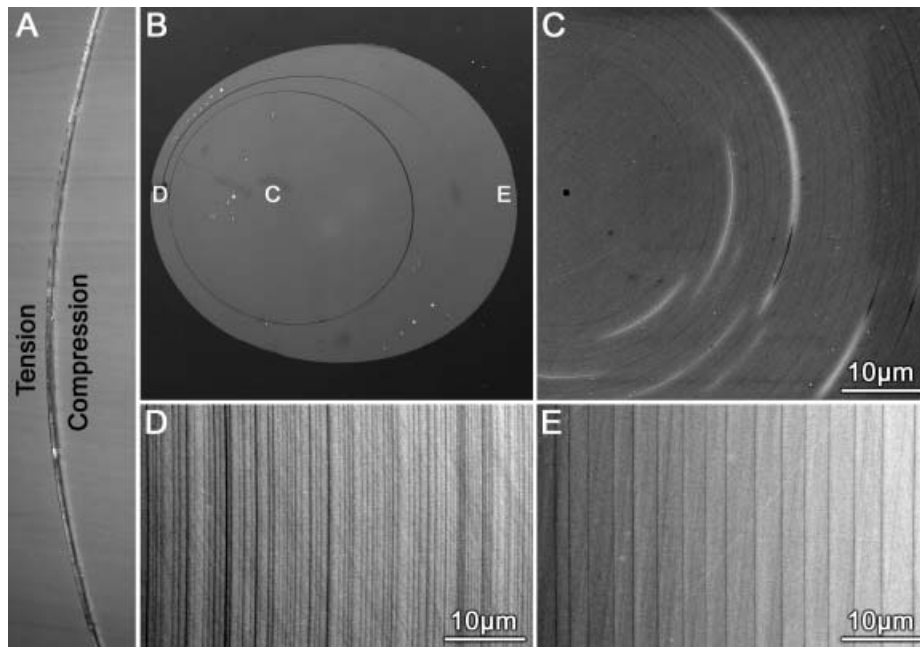
The objective of the present study was to ascertain the role of the laminate architecture in the fracture resistance of the giant anchor spicule of *M. chuni*. This species was selected because of its unusually large size, thus permitting use of established indentation techniques that would otherwise be restricted by specimen dimensions. To provide a basis for comparison, tests have been performed on both the laminated cortex and the homogeneous core (an ideal control material), as well as a fused quartz standard.

Pertinent details of the spicule microstructure are reviewed in Section 2. Indentation fracture data are described in Section 3, beginning with the underlying theory of deformation and cracking at sharp indents. As is evident in the following development, the theory is essential to both the design of the experimental program and the subsequent data analysis. This is followed by a detailed account of the experimental measurements and observations. Conclusions and implications are summarized in the final section.

2. Spicule Microstructure

M. chuni spicules used in this study were collected from Lifou (Loyalty Island, New Caledonia, South Pacific Ocean) and Norfolk Ridge (South Pacific Ocean). The main structural features are summarized in Figures 2 and 3. The central core consists of monolithic hydrated silica and is surrounded by a series of concentric rings of silica and very thin (ca. 10 nm) intervening layers of proteinaceous material. The volume fraction of organic material is extremely small, of the order of 1%. As reported previously by Schulze,[8] and confirmed by our present studies, there is a distinct asymmetry in the silica layer thickness on the tensile and compressive sides of the spicule, likely a response to predominantly unidirectional bending loads. While most clearly seen in spicules of greater than 1 m in length (Figs. 2B–E and 3A), asymmetry has also been reported for smaller spicules from the same sponge species (Fig. 3C and D).

In some instances, large spicules (greater than 2 m in length) develop an elliptical cross-section, with the major axis of the ellipse coinciding with the direction of curvature (Fig. 3A). The ratio of bending strengths of elliptical and circular sections with the same area is given by the section shape factor $\phi = a/b$ where a and b are the major and minor axes, respectively.[11] For the example in Figure 3A, $\phi \approx 12$. The implication is that a spicule with an elliptical cross-section would be 20% stronger

Figure 1. Anchor spicule diversity in hexactinellid sponges. While many sediment-dwelling hexactinellids such as *Semperella cucumis* (left) secrete hundreds to thousands of small fibrillar anchor spicules, *Monorhaphis chuni* (right) secretes a single giant anchor spicule that secures the sponge into the sea floor (Adapted from [8]).

(Fig. 1).[9] These spicules are usually curved, because of the bending loads imposed by the prevailing ocean currents (Fig. 2A).[6] As first reported by Schulze in his studies of *M. chuni* specimens collected during the Valdivia expedition of the late 1800s (Fig. 3C–D), the silica is frequently distributed asymmetrically around the spicule perimeter, with the layer thickness on the tensile side being significantly less than that on the compressive side.[8] In light of the scaling of the tensile cracking stress with $h^{-1/2}$, the growth asymmetry further supports the notion of an adaptation for increased strength.

The laminate architecture also suggests an adaptation for enhanced *toughness*. Provided the proteinaceous material

Figure 2. Structural details of the *M. chuni* anchor spicule. (A) Portion of one of the spicules used in this study, revealing its curvature and the tensile and compressive sides. (B) Low magnification BSE image of the spicule cross-section revealing section asymmetry. The main regions include a solid cylindrical core (C) surrounded by ca. 15 μm thick silica layers and thin exterior surface layers on the tensile (D) and compressive sides (E). Locations of C–E are indicated on (B).

variations in microstructure over short distances. Additionally, with the advent of instrumented nanoindenters, the methodology simultaneously provides information on the resistance to plastic deformation (characterized by hardness) as well as the stiffness (characterized by the Young's modulus). Equally importantly, indentation allows for the study of both crack initiation *and* propagation — a feature exploited in the present study.

Indentation tests are most commonly performed using a diamond indenter with Vickers, Berkovich, or cube-corner geometry. Each consists of three or four flat faces that intersect at the indenter tip and produce a corresponding number of sharp edges. During the loading phase, a plastic indent is formed with a characteristic dimension, measured from the indent center, given by

$$a = \left(\frac{P}{\alpha H} \right)^{1/2} \tag{1}$$

in bending than one with a circular section of equal area. This feature is again suggestive of a growth adaptation, in this case for efficient utilization of available material to meet structural requirements.

Additionally, the large spicules exhibit a high degree of asymmetrical silica deposition. The layer thickness on the compressive face decreases exponentially with layer number (measured from the spicule center) over the entire growth history, from approximately 10 to 2 μm (Fig. 3B). The layer thickness on the tensile face also diminishes exponentially with layer number, but at a significantly higher rate (Fig. 3B), eventually reaching a value of about 0.6 μm after 250–300 layers have been deposited. The thickness of each of the remaining (outermost) 200 layers is the same, typically 10–20% of that of the corresponding layer on the compressive side. The focus of the present study is on the former (finely laminated) architecture.

3. Indentation
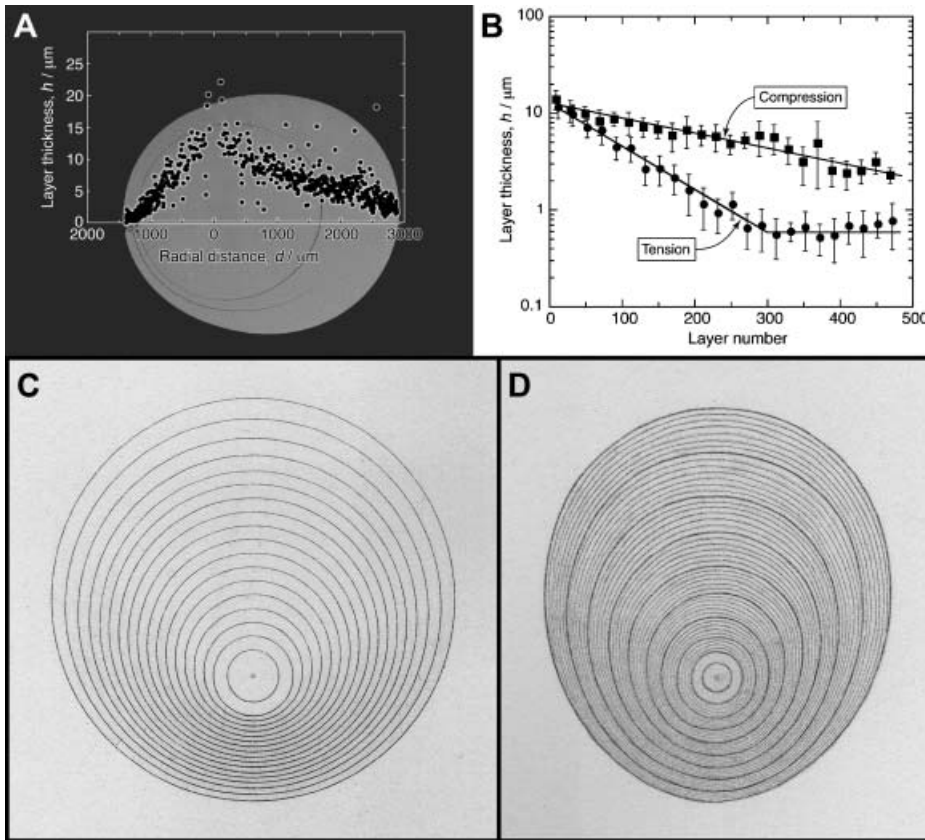
3.1. Mechanical Theory

Indentation is widely used for evaluating the fracture resistance of brittle solids and is the most viable option for probing small volumes of material or materials that exhibit

where P is the peak load, H is the hardness, and α is a nondimensional geometric parameter ($\alpha = 2$ for the four-sided Vickers indenter and 1.30 for the three-sided Berkovich and cube-corner indenters). When P is sufficiently high (defined below), plasticity is accompanied by radial cracks that emanate from the indenter edges and extend with increasing load. Residual stresses that develop during unloading cause the cracks to extend further at the surface, with the final crack length (also measured from the indent center) given by[12]

$$c = \left(\frac{E}{H} \right)^{1/2} \left(\frac{\chi P}{K_c} \right)^{2/3} \tag{2}$$

where E is Young's modulus, K_c is the fracture toughness and χ is a nondimensional constant (0.022 for Vickers and Berkovich indenters and 0.040 for cube-corner indenters[13]). The residual field can also cause lateral (saucerlike) cracks directly beneath the indenter parallel to the free surface. Because of their orientation, lateral cracks are not visible on the surface of opaque materials.

Since the radial crack length exhibits a stronger sensitivity to the load than that of the indent size (manifested in the power law exponents 2/3 and 1/2 in Eqs. 1 and 2), a critical load P_c exists, below which the predicted crack length is smaller than the indent size. Physically, this point represents an initiation

Figure 3. (A) Plot of silica layer thickness against distance from the spicule center in the direction of bending, illustrating the asymmetry in the tensile and compressive regions. The background image is a backscattered scanning electron micrograph of the examined cross-section. The location indicated by "0" on the abscissa denotes the location of the spicule core. (B) Variation in silica layer thickness with layer number (measured from the spicule center) at both the tensile and the compressive sides of the spicule. Each datum point is the average of 20 measurements and the error bars represent one standard deviation. (C) and (D) illustrate cross-sections of smaller *M. chuni* anchor spicules measuring 47 μm and 78 μm in diameter across the long dimension, respectively. These illustrations (adapted from [8]) reveal that the asymmetry in silica layer thickness can begin quite early in the stages of spicule formation, likely in response to unidirectional bending loads.
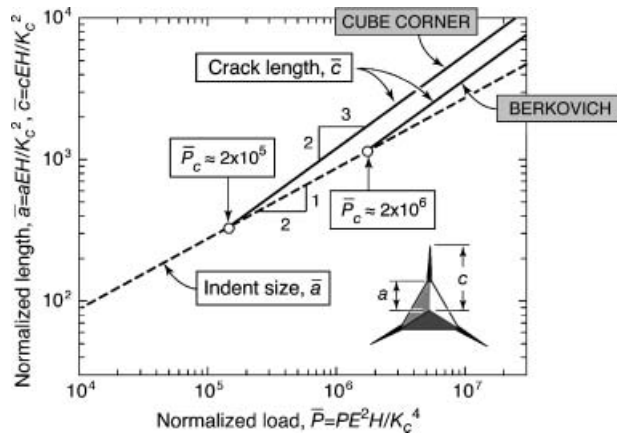
The latter results can be used to construct a universal diagram of indentation deformation and fracture for a specified indenter geometry (characterized by α and χ). Two such examples, for cube-corner and Berkovich indenters, are presented on Figure 4. Of the two indenter geometries, cube corner exhibits the greater propensity for radial cracking. That is, the intersection of $\overline{a}(\overline{P})$ and $\overline{c}(\overline{P})$ for the cube-corner indenter occurs at a load an order of magnitude lower than that for the Berkovich indenter ($\overline{P}_c \approx 2 \times 10^5$ vs. 2×10^6), consistent with experimental findings.[13–15] The threshold for the Vickers indenter occurs at an intermediate load. Because of these trends, the cube-corner indenter was employed in the present experimental study.

3.2. Indentation Results

Hardness and modulus measurements are summarized in Figure 5. The trends with load P for the fused-quartz standard (including the slight but noticeable hardness peak at $P \approx 10$ mN) are comparable to those reported earlier.[16,17] The average values over the load range employed in the present study are $E \ap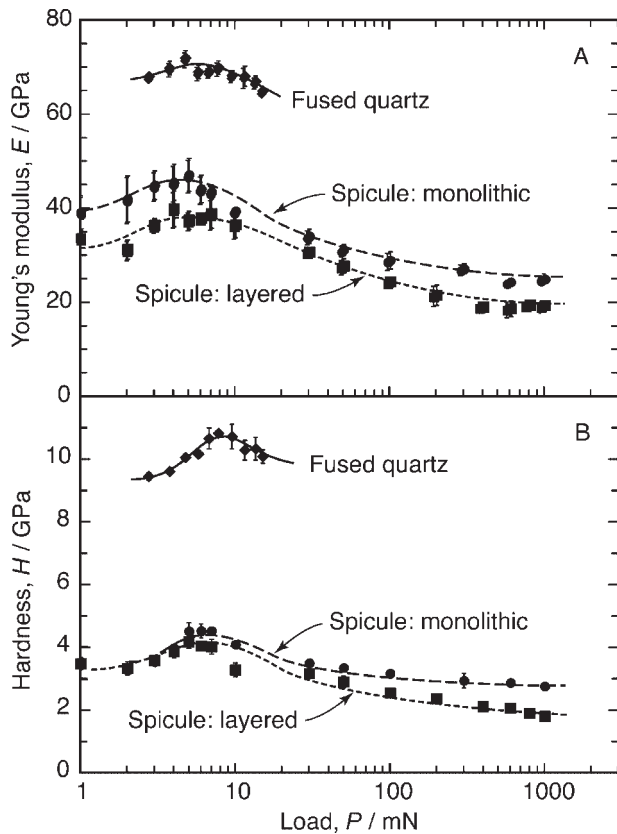prox 68$ GPa and $H \approx 10$ GPa. Both E and H for the silica from the spicule core are only about half of the respective values for the fused quartz, a difference attributed to the hydrated nature of the silica in the spicules.[3,5] The properties of the laminated region are lower yet, by 10–20%: an effect attributable to the softer proteinaceous material and the damage that accompanies indentation.

Despite similarities in their modulus and hardness, the laminated regions and the monolithic core exhibit dramatically different fracture properties. In the latter, cracks form readily at indent corners at all but the very lowest indentation loads and subsequently propagate outward along radial planes (Figure 6A). This behavior is virtually identical to that in other brittle solids, including the fused quartz tested here. Subsequent ultrasonication causes removal of a scallop-shaped piece of material around the indentation site, presumably due to lateral cracks that formed during the unloading phase of indentation as well as the radial cracks that link the lateral cracks to the free surface (Figure 6B). The spatial extent of material removal is of the order of $2c$. In contrast, the

threshold. That is, cracks can form at the indent corners only when $P > P_c$. An estimate of P_c is obtained by setting $a = c$, whereupon

$$P_c = \frac{1}{\alpha^3 \chi^4} \frac{K_c^4}{E^2 H} \tag{3}$$

The preceding results can be re-expressed in terms of three non-dimensional parameters, representing indent size, $\overline{a}$, crack length, $\overline{c}$, and load, $\overline{P}$, defined by:

$$\overline{a} \equiv \frac{aEH}{K_c^2}, \quad \overline{c} \equiv \frac{cEH}{K_c^2}, \quad \overline{P} \equiv \frac{P E^2 H}{K_c^4} \tag{4}$$

With these definitions, Eqs. 1–3 are re-written as

$$\overline{a} = \left(\frac{\overline{P}}{\alpha}\right)^{1/2}, \quad \overline{c} = (\chi\overline{P})^{2/3}, \quad \overline{P}_c = \frac{1}{\alpha^3 \chi^4} \tag{5}$$

Figure 4. Universal indentation deformation/fracture diagram, constructed using normalized parameters defined in Eqn. 4 and the relationships in Eqn. 5. The intersection points of the lines representing $\bar{a}(\bar{P})$ and $\bar{c}(\bar{P})$ define the cracking threshold loads, $\bar{P}_c$.

laminated region exhibits a more damage tolerant response. Notably, at low and moderate loads indents are accommodated by the plasticity of the constituent silica and sliding of the silica layers past one another via shear of the intervening proteinaceous material. Some material removal occurs during subsequent ultrasonication, but the spatial extent is limited to a

Figure 5. Effects of indentation load on (A) Young's modulus and (B) hardness of monolithic and laminated regions of the spicule as well as the fused quartz standard. Each datum point is the average of 6–10 measurements.

distance of about $2a$ (compare Figs. 6B and 7D). Cracking across the silica layers ahead of the indent corners occurs only at the highest indentation loads (Figure 7B).
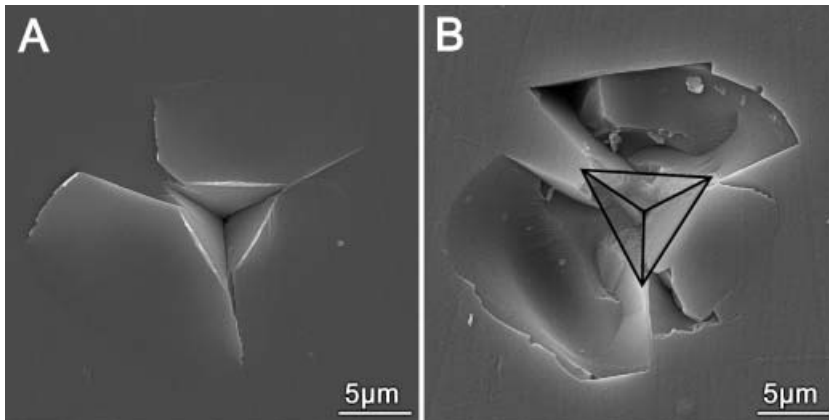
The resistance to crack initiation was assessed in terms of the cumulative frequency of cracking, which is defined by the ratio of the total number of radial cracks to the number of possible initiation sites (three per indent). In the monolithic silica, the presence or absence of radial cracks could be readily ascertained from scanning electron microscopy (SEM) images of each of the three indent corners. In the laminated regions, only those edges oriented roughly perpendicular to the layers and generating nominally mode I (opening) cracks were considered in this assessment. Furthermore, in the latter case, radial cracks were deemed to have formed only if they had traversed across the organic layer immediately ahead of the indent corner and renucleated in the next silica layer. In total, about 200 indents were examined. The results are plotted in Figure 8. The initiation loads, defined at 50% cracking frequency, differ by about two orders of magnitude: $P_c \approx 5$ and $500\,\text{mN}$ for the monolithic and laminated silica, respectively. Clearly, the laminate architecture is extremely effective in mitigating the propensity for crack formation at sharp indents. The threshold load for the fused quartz was found to be comparable to that of the monolithic silica, falling in the range of 5–7 mN, with 100% cracking frequency for $P \geq 8$ mN.

Crack-length measurements (for $P > P_c$) are summarized in Figure 9A. To ascertain the fracture toughness, K_c, the crack length measurements have been replotted in Figure 9B as $c^{3/2}(H/E)^{1/2}$ vs. P, as suggested by the functional form of Eq. 2, using the measured values of E and H. A least-squares regression analysis of the data for fused quartz yields $K_c = 0.53\,\text{MPa}\sqrt{\text{m}}$: essentially the same as that reported for a similar quartz material, measured by chevron-notched bend tests ($K_c = 0.58\,\text{MPa}\sqrt{\text{m}}$).[13] The two spicule materials exhibit fracture toughness values on either side: $K_c = 0.35$ and $0.84\,\text{MPa}\sqrt{\text{m}}$ for the monolithic and laminated silica, respectively. The latter difference in K_c is directly attributable to the laminate architecture.

Finally, the experimental results for the three materials have been plotted on a universal indentation deformation/fracture diagram, using the normalizations defined in Eq. 4 (Figure 10). In this form, the data collapse into essentially a single pair of lines, consistent with the theoretical predictions (Eq. 5). The implications are discussed below.

4. Discussion and Conclusions

In light of the very small volume fraction of proteinaceous material in the *M. chuni* spicule (<1%), the corresponding enhancement in fracture resistance (by a factor of 2.5) is remarkable. This is believed to be due largely to the process of crack deflection within the organic layers, similar to that which occurs in other tough biomaterials, for example, nacre.[19] Regardless of whether deflection occurs by debonding and subsequent sliding at the interfaces or by plasticity within the

Figure 6. SEM images of (A) residual indent and radial cracks in monolithic spicule after indentation to 100 mN and (B) the same region after ultrasonication, revealing the extent of local damage. Outlined triangle in (B) represents the location of the initial indent in (A).

interlayer, theoretical analyses and numerical simulations[7,18] have shown that significant reductions in crack-tip stresses can be obtained, thereby increasing composite toughness.
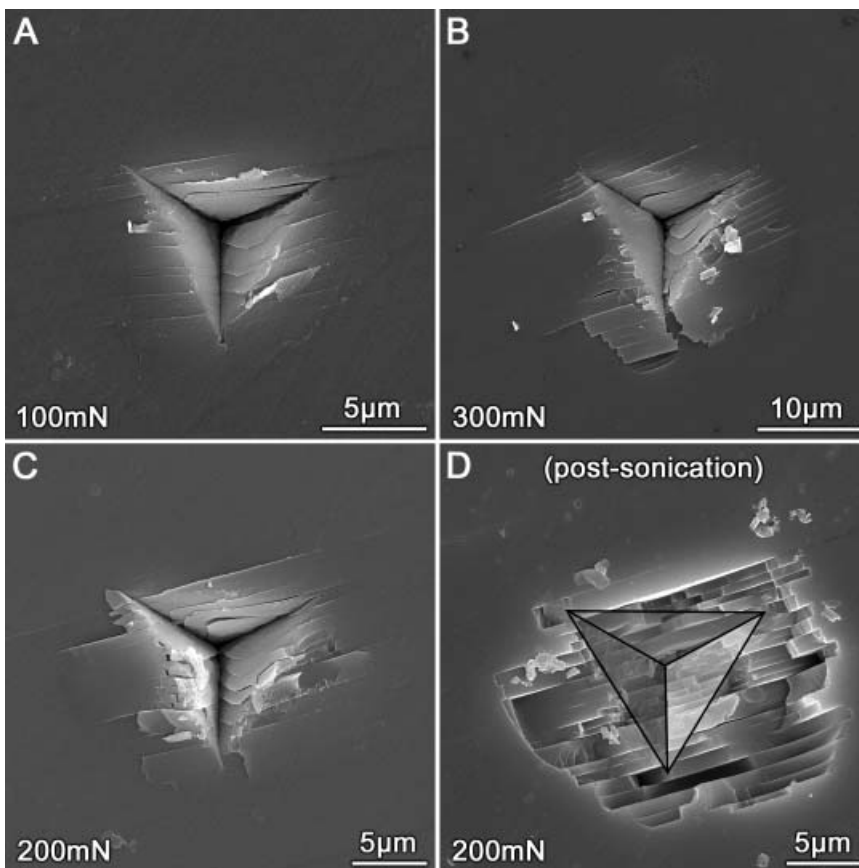
Additional perspective on the increase in fracture resistance is obtained through comparisons with the properties of engineered glass matrix composites. A common strategy for toughening involves the addition of fine, well-bonded metallic particles. Studies have been performed with Ni,[20] Cu,[21] Mo,[22] and Al.[23] Enhancement of the toughness is derived from plastic stretching of the particles in the wake of an advancing matrix crack. However, even under the most favorable circumstances, where the particles exhibit high yield stress and ductility and remain bonded to the matrix, a twofold increase in fracture toughness requires the addition of 10–20% metal reinforcement: more than an order of magnitude greater than the protein fraction in the *M. chuni* spicules. Analogous toughening mechanisms can be activated in brittle polymers, such as epoxies, through the addition of rubber particles. Although more effective than the glass/metal systems, rubber volume fractions of at least 5% are needed to achieve a comparable twofold increase in fracture toughness.[24]
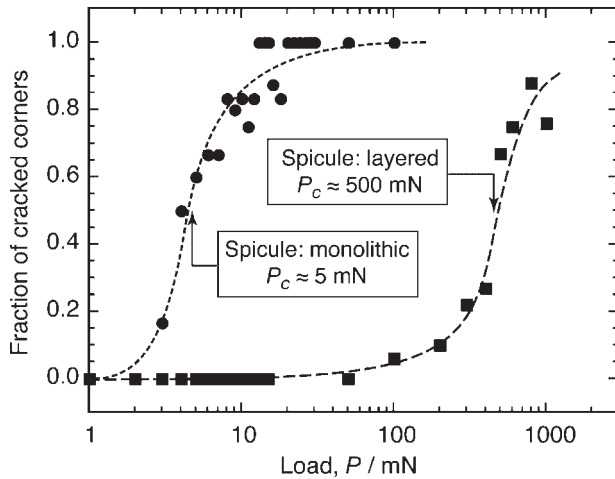
The 100-fold increase in the threshold load for crack initiation is equally impressive. Its origin, in terms of the fundamental mechanical properties E, H and K_c, is evident from the scaling in Eq. 3: $P_c \propto K_c^4/E^2H$. Comparing the properties of the laminated and the monolithic silica in the spicule reveals that the threshold difference is dominated by K_c. That is, with the ratio of fracture toughnesses being about 2.5, the ratio of threshold loads is predicted to be $2.5^4 \approx 40$ (assuming constant E and H). Modulus and hardness differences play a decidedly minor role. With E and H values for the laminated material being about 80% of those of the monolithic material, the corresponding increase in the predicted threshold load is a factor of $0.8^{-3} \approx 2$. Thus, the *combined* effects of changes in E, H, and K_c result in a threshold increase of a factor of 80, broadly consistent with the experimental measurements (Fig. 8).

The results also provide insights into the damage tolerance of the monolithic silica within the spicules relative to fused quartz. Interestingly, the reduction in the threshold load of the silica due to its lower fracture toughness is offset by reductions in H and E, resulting in little change in the quantity K_c^4/E^2H. This prediction is consistent with the similar threshold loads obtained for hydrated silica and quartz in the present study. One inference is that the replacement of the inorganic phase of the laminate with
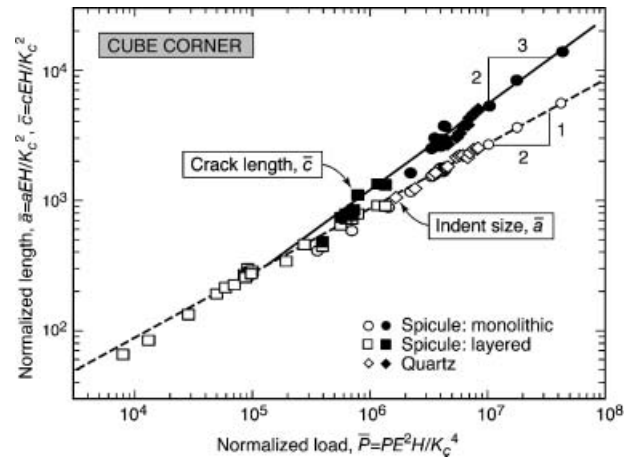

Figure 7. (A–C) SEM images of indents and local damage in the laminated regions of the spicule after indentation to loads of 100–300 mN. (D) Same region as in (C), after ultrasonication. Outlined triangle in (D) represents location of the indent in (C).

Figure 8. Cracking frequency in monolithic and laminated regions of the M. chuni spicule.

Figure 10. Universal indentation deformation/fracture diagram, constructed using experimental data obtained from the present study.

an alternate form of silica, with higher modulus and hardness, may not yield an improvement in the cracking threshold. This also opens the possibility of a natural growth adaptation in which the composition of the constituent silica has been modified to confer an optimal balance of hardness and stiffness, yielding the requisite fracture resistance when present in laminated form with the organic material.
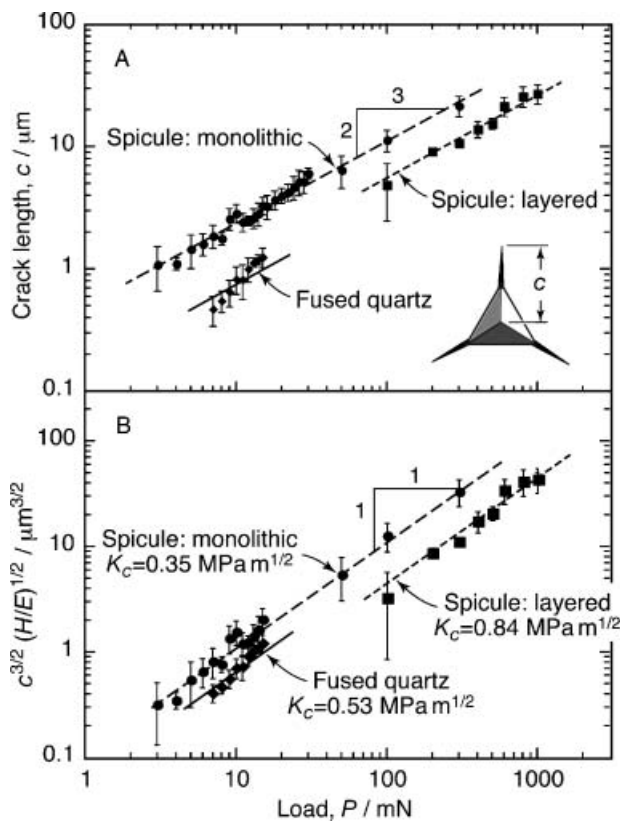

Figure 9. (A) Effects of indentation load, P, on crack length, c. (B) Determination of fracture toughness, from the variation in $c^{3/2}(H/E)^{1/2}$ with P.

Finally, it is important to note that the natural conditions encountered by the spicules in the deep sea differ from those employed in the laboratory and may influence the material properties. Perhaps most important in this regard is the effect of hydration. Although the plasticization normally associated with hydration decreases the resistance to both elastic and plastic deformation and increases the toughness,[19,25] the magnitude of these effects in the spicules is expected to be smaller than that encountered in other biological tissues. Two supporting observations are most relevant. First, because water is chemically bound to the spicule silica, the structure is expected to remain hydrated even in ambient air. This assertion is supported by NMR measurements (unpublished) and is consistent with the twofold reduction in the measured modulus and hardness of the spicule material at the core relative to those of pure silica (quartz). Second, provided suitable pathways for water ingress through the silica were available, hydration effects would be greatest in the organic interlayers. The concentric arrangement of the two constituents, however, precludes direct access of water to the inner organic layers. Diffusion through the silica would ultimately control the rate of ingress. If this process did indeed occur, it would have the effect of reducing E and H and increasing K_c of the composite material. In turn, the threshold cracking load would be elevated in accordance with the scaling $P_c \propto K_c^4 / E^2 H$.

5. Experimental

Specimens: *M. chuni* anchor spicules used in this study were collected at a depth of 1905 m near Lifou (Loyalty Island), New Caledonia during the CALSUB campaign in 1989 and from Norfolk Ridge at a depth of 1200 m during the HALIPRO campaign in 1996. Spicule segments were embedded in M-Bond AE-15 (M-Line, Raleigh N.C.) epoxy, sliced into 3 mm thick transverse sections using a diamond cutting wheel, and polished with diamond lapping films with particles sizes down to 0.1 μm under a constant flow of fresh water. Both sides of the sectioned region were polished; one side was imaged uncoated in an

environmental scanning electron microscope, and the other was used for the indentation studies.

Scanning Electron Microscopy: Embedded samples were examined uncoated using the backscattered electron (BSE) detector of a FEI XL-30 environmental scanning electron microscope. For measuring individual silica layer thickness (Figure 2), a series of overlapping BSE images were acquired at a constant magnification across the entire spicule diameter; the resulting 121 individual images were combined into a single data file, and the layer thickness and spicule radius were determined and plotted using IDL (Research Systems Inc., Boulder, CO, USA) and ProFit (Quantum Soft, Uetikon am See, Switzerland). *Nanoindentation*: The samples were prepared using the same technique described above. Indentation tests were performed in ambient air using a Triboscan nanoindenter system (Hysitron, Minneapolis, MN, USA) with cube-corner diamond tips. The primary focus was on the laminated regions near the tensile surface of the spicule and the monolithic core. Additionally, to provide perspective on the properties of the silica core, tests were also performed on a fused quartz standard. Peak indentation loads were varied from 1 to 1000 mN, using a 30 mN transducer (for load range 1 to 30 mN) and a Multi Range Nano Probe (maximum load 1000 mN) for higher load indents. Hardness and Young's modulus were calculated from the unloading portions of the load-displacement curves following established procedures. [26] After indentation, the samples were sputter-coated with gold and examined by SEM. Low load indents were imaged with a FEI XL-40 field emission gun allowing imaging at higher magnification, while larger load indents were observed with a Tescan Vega TS5130-MM thermionic emission SEM. These examinations were used to measure the size of both the indents and the cracks (when present). The samples were subsequently placed in an acetone bath, ultrasonicated, and re-examined in the SEM. Removal of debris and other weakly-attached fragments from the indentation site allows complementary information about subsurface damage to be gleaned from the SEM observations.

[1] J. Aizenberg, J. C. Weaver, M. S. Thanawala, V. C. Sundar, D. E. Morse, P. Fratzl, *Science* **2005**, *309*, 275.

[2] J. C. Weaver, J. Aizenberg, G. E. Fantner, D. Kisailus, A. D. Woesz, P. Allen, K. Fields, M. J. Porter, F. W. Zok, P. K. Hansma, D. E. Morse, *J. Struct. Biol.* **2007**, *158*, 93.

[3] A. Woesz, J. C. Weaver, M. Kazanci, Y. Dauphin, J. Aizenberg, D. E. Morse, P. Fratzl, *J. Mater. Res.* **2006**, *21*, 2068.

[4] S. L. Walter, G. Mayer, B. D. Flinn, *Mater. Sci. Eng., C*, **2007**, *27*, 570.

[5] M. Sarikaya, H. Fong, N. Sunderland, B. D. Flinn, G. Mayer, A. Mescher, E. Gaino, *J. Mater. Res.* **2001**, *16*, 1420.

[6] C. Levi, J. L. Barton, C. Guillemet, E. Le Bras, P. Lehuede, *J. Mater. Sci. Lett.* **1989**, *8*, 337.

[7] J. W. Hutchinson, Z. Suo, *Adv. Appl. Mech.* **1992**, *29*, 63.

[8] F. E. Schulze, *Hexactinellida. Wissenschaftliche Ergebnisse der Deutschen Tiefsee-Expedition auf dem Dampfer ''Valdivia'' 1898–1899*, Verlag Gustav Fischer, Jena Germany **1904**.

[9] C. Chun, *Aus den Tiefen des Weltmeeres*, Verlag Gustav Fischer, Jena Germany **1900**.

[10] W. J. Clegg, K. Kendall, N. M. Alford, T. W. Button, J. D. Birchall, *Nature* **1990**, *347*, 455.

[11] M. F. Ashby, *Materials Selection and Process in Mechanical Design*, 3rd ed., Butterworth–Heinemann, Oxford, UK **2005**, p. 624.

[12] B. Lawn, *Fracture of Brittle Solids*, 2nd ed., Cambridge University Press, Cambridge, UK **1993**, 378.

[13] G. M. Pharr, *Mater. Sci. Eng., A* **1998**, *A253*, 151.

[14] D. S. Harding, W. C. Oliver, G. M. Pharr, *Mater. Res. Soc. Symp. Proc.* **1995**, *356*, 663.

[15] D. J. Morris, R. F. Cook, *J. Am. Cer. Soc.* **2004**, *87*, 1494.

[16] J. A. Knapp, D. M. Follstaedt, S. M. Myers, J. C. Barbour, T. A. Friedman, *J. Appl. Phys.* **1999**, *85*, 1460.

[17] K. Ikezawa, T. Maruyama, *J. Appl. Phys.* **2002**, *91*, 9689.

[18] K. S. Chan, M. Y. He, J. W. Hutchinson, *Mater. Sci. Eng., A* **1993**, *A167*, 57.

[19] F. Barthelat, H. D. Espinosa, *Exper. Mech.* **2007**, *47*, 311.

[20] D. J. Green, P. S. Nicholson, J. D. Embury, *J. Mater. Sci.* **1979**, *14*, 1413.

[21] G. Banuprakash, V. Katyal, V. S. R. Murthy, G. S. Murty, *Composites A* **1997**, *28*, 861.

[22] I. Dlouhy, M. Reinisch, A. R. Boccaccini, J. F. Knott, *Fatigue Fract. Eng. Mater. Struct.* **1997**, *20*, 1235.

[23] E. Bernardo, G. Scarinci, S. Hreglich, *J. Europ. Ceram. Soc.* **2003**, *23*, 1819.

[24] K. P. Unnikrishnan, E. T. Thachil, *Designed Monomers and Polymers* **2006**, *9*, 129.

[25] D. Zhang, A. Nazari, M. Soappman, D. Balaj, D. Arola, *Exper. Mech.* **2007**, *47*, 325.

[26] W. C. Oliver, G. M. Pharr, *J. Mater. Res.* **1992**, *7*, 1564.